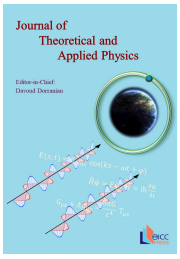

Volume 17, Issue 1, 172309 (1-9)

Journal of Theoretical and Applied Physics (JTAP)

https://dx.doi.org/10.57647/j.jtap.2023.1701.09

Laser ablation produced graphene/MOF-5 nanocomposite: antibacterial properties

Negar Motakef-Kazemi [1]*, Fereydoon Ataei[2], Davoud Dorranian[2]

[1]*Department of Medical Nanotechnology, Faculty of Advanced Sciences and Technology, Tehran Medical Sciences, Islamic Azad University, Tehran, Iran.*
[2]*Laser Lab., Plasma Physics Research Center, Science and Research Branch, Islamic Azad University, Tehran, Iran.*

*__Corresponding author__: motakef@iaups.ac.ir

Received 4 July 2022; Accepted 29 November 2022; Published online 3 December 2022

Abstract:
Preparation of graphene decorated MOF-5 nanocomposite by pulsed laser ablation (PLA) method in liquid environment has been investigated for the first time. Firstly, MOF-5 nanostructures were synthesized by irradiating a high-purity zinc (Zn) plate in dimethylformamide (DMF) solution containing terephthalic acid ligand with Nd:YAG pulsed laser. Using the fundamental wavelength of Nd:YAG laser at 1046 nm and pulse width of 7 ns, three samples of MOF-5 nanostructures were produced in the solutions with three ligand concentrations. Then, by laser ablation of a graphite target in the MOF-5 nanostructures suspensions, graphene/MOF-5 nanocomposites were produced. Furthermore, the antibacterial activity of the samples was evaluated against Escherichia coli (*E. coli*) as a gram-negative and Staphylococcus aureus (*S. aureus*) as a gram-positive bacterium. Morphology of MOF-5 nanostructures was modified due to presence of graphene nanosheets in the structure of nanocomposite. TEM images show that square shape MOF-5 particles were located on the surface of graphene nanosheets. Concentration of synthesized samples was increased with increasing the ligand concentration in the liquid environment of ablation. And stronger antibacterial effects of nanocomposites were observed against the gram-negative bacteria due to their gravitation of opposite charges.

Keywords: Graphene; Laser ablation; Metal–organic framework; MOF-5; Nanocomposite

1. Introduction

Metal–organic frameworks (MOFs) are porous hybrid organic-inorganic materials as the coordination polymers [1, 2]. In recent years, MOFs have attracted much attention due to their large surface area, high pore volume, and adjustable shape and pores [3, 4]. MOFs are used in different applications such as drug delivery, nonlinear optics and optoelectronic devices, polymers modification, Raman scattering, sensors, photocatalysis, gas storage, composite, photoluminescence, nanoparticle preparation, sorbent, and antibacterial researches [5–22].
There are several methods to synthesize MOFs including self-assembly metal clusters as the metal centers and organic ligands as linkers using various methods such as solution, solvothermal, hydrothermal, mechanochemical, electrochemical, microwave, sonochemical, diffusion, ionic liquids, and laser ablation methods [23–36].
MOF-5 is the most common zinc-based metal organic framework, which was introduced by Omar Yaghi in 1999. This MOF was synthesized by connection of Zn4O units and 1,4-benzenedicarboxylate ligands to form a cubic network with the formula $Zn_4O(BDC)_3$. MOF-5 nanostructures also have a wide range of applications including drug delivery, Raman scattering, nitrate adsorption, gas absorption, catalysis, gas storage, electrochemical activity, diffusion, molecular sensing, electronic and vibrational properties, as well as antibacterial agents [37–53].
So far, the reported methods to synthesize MOF-5 nanostructures are solvothermal, microwave, microwave hydrothermal, electrochemical, sonochemical, solution, ionic liquid microemulsion, mechanochemical, ultrasound and microwave, and laser ablation methods [54–63].
The capability of CW and pulsed lasers in processing materials and specially the role of laser in the production and modification of nanomaterials have been investigated frequently. PLA is an environmentally friendly green method with high purity nano products. Variety of controlling tools

such as laser fluence, wavelength, pulse width, and spot size is the most important advantage of PLA method to process nanomaterials [64–71]. Employing PLA method to produce Bi-MOF and MOF-5 was first introduced in our former reports [36, 64]. In that work MOF-5 was synthesized by laser ablation of Zn target in dimethylformamide solution, containing terephthalic acid. In this study, decoration of graphene nanosheets by MOF-5 nanostructure has been reported for the first time.

Graphene is an allotrope of carbon consisting of a single layer of atoms arranged in a two-dimensional honeycomb lattice nanostructure. Each atom in a graphene sheet is connected to its three nearest neighbors by a strong σ-bond, and contributes to a valence band one electron that extends over the whole sheet. This unique structure has led to unique properties in this sheet of carbon. It has been demonstrated that the presence of small amounts of nanostructures in close contact with the graphene nanosheets forms a heterojunction that can improve the photocatalytic activity of composition noticeably. The most widely accepted mechanism to explain the improvement in the photocatalytic activity of these hybrid systems is related to charge transfer from the semiconductor conduction band minimum graphene nanosheet. The high electron mobility in graphene determines that, once the electron is on graphene, they become delocalized through the sheet. In that way, the close contact between nanostructure and graphene favors photoinduced charge separation and catalytic activities [72].

Following lots of challenges to synthesize graphene and graphene oxide nanosheets, laser ablation method has been found to be one of the best. Furthermore, laser ablation method has been found to be a capable method to produce decorated graphene nanosheets by conductor and semiconductor nanostructures [73–80]. In this paper, the first experimental challenge for production of graphene/MOF-5 nanocomposites by PLA method is reported. Results show that pulsed laser ablation is a promising method to synthesis different form of graphene-MOF nanocomposites.

2. Experimental Section

2.1 Materials

Materials including zinc metal target for preparation of Zn^{2+} ion as a connector center, 1,4 benzenedicarboxylic acid (BDC) as a bridging ligand, and dimethylformamide (DMF) as a solvent were purchased from Merck (Darmshtadt Germany).

2.2 Synthesis

MOF-5 was prepared by laser ablation technique via the self-assembly at room temperature based on previous report [64]. The zinc target was placed in a Beaker with 40 ml of DMF solvent solution containing 0.328, 0.631, and 1.234 g of BDC ligand, labeled as samples a, b, and c respectively. The target was irradiated with 1500 pulses of the fundamental wavelength of a pulsed Nd:YAG laser (Quantel, model Brilliant B) with 1064 nm wavelength, operating at 5 Hz repetition rate and 7 ns pulse width with 0.7 J/cm^2 fluence under magnet stirring. The laser beam with a diameter of 6 mm was focused on the surface of the target using a 10 cm focal length convex lens. The height of the liquid on the target surface was 5 mm during the ablation process. To produce the graphene/MOF-5 nanocomposite, a graphite plate was irradiated by 1500 pulses of the same laser in the produced MOF-5 nanostructures suspensions. Finally, 3 samples of graphene/MOF-5 nanocomposite were synthesized with different concentration of BDC ligand in 40 mL of DMF solvent. As soon as the ablation started, the solution color was changed and a solid precipitation occurred.

2.3 Characterization

Graphene/MOF-5 nanocomposites were characterized by FTIR, XRD, FESEM, TEM, and UV–vis spectroscopy. Fourier transform infrared spectra were recorded on a Spectrum Two spectrometer (PerkinElmer) in a KBr matrix. UV–Vis spectroscopy was done for investigation optic properties (Shimadzu, UV-2550, Japan). X-ray diffraction measurements were performed using a X′ Pert Pro diffractometer (Panalytical, Netherlands) for evaluation of crystalline structure. The morphology of nanocomposites was recorded by size field emission scanning electron microscope (Zeiss-SIGMA VP, Germany) with gold coating. Also, transmission electron microscope (Zeiss, EM10C-100 kV, Germany) was employed for presentation of morphology and size of synthesized graphene/MOF-5 nanostructures.

2.4 Antibacterial activity

Minimum bactericidal concentration (MBC) and minimum inhibitory concentration (MIC) were used to study the antibacterial activities of synthesized nanostructures against Escherichia coli as a gram-negative bacteria (ATCC 25922) and Staphylococcus aureus as a gram-positive bacteria (ATCC 25923). Muller Hinton Agar solid culture medium was used for microbial tests. This environment was prepared according to the Merck manufacturer's agenda. The amount of 34 g of culture medium powder was dissolved in 1 liter of distilled water and then boiled with gentle heat for 1 minute. After preparing a uniform and clear solution, it was sterilized in an autoclave at 121 ℃ for 15 minutes and then cooled to 45-50 ℃. The amount of 50 ml of it into each sterile plate and let it cool at room temperature. In order to standardize the concentration of microbial liquid for testing, a standard turbidity should be used. The turbidity standard is made with barium sulfate equivalent to half McFarland standard or its optical equivalent can be used by photometry. The amount of microbial culture needed to perform microbial tests is 1 ml of liquid culture medium, which contains 1-2×108 bacteria. In other words, the turbidity of bacteria leachate is suitable in the logarithmic phase, which is similar to McFarland half tube, is suitable. Then, the bacterial suspension was cultured in half of McFarland's medium with sterile swap on Mueller Hinton agar culture medium. Finally, the discs impregnated with samples, which were prepared by immersion, were placed in the plate with a suitable distance. The plate was placed in an incubator at 37 ℃ for 24 h. Broth microdilution method was used for the MIC test. First, the tested antibacterial substances were accurately weighed and dissolved in 1 ml of sterile distilled water and the initial stock was prepared. In the

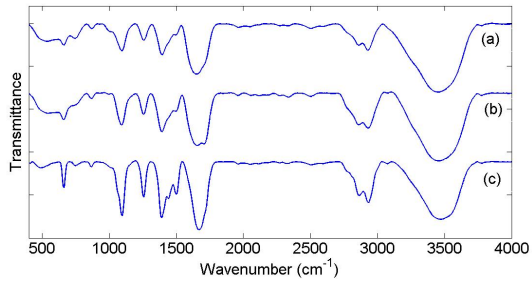

Figure 1. FTIR spectra of graphene/MOF-5 nanocomposites at different BDC ligand concentrations a) 0.328, b) 0.631, and c) 1.234 g.

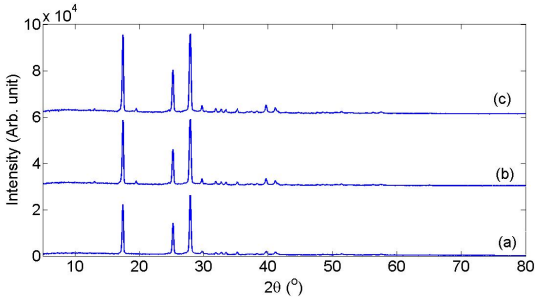

Figure 2. XRD patterns of graphene/MOF-5 nanocomposites at different BDC ligand concentrations a) 0.328, b) 0.631, and c) 1.234 g.

next step, the experiment was performed using the microdilution method in a sterile 96-well microplate. The steps of the experiment were as follows: First, 100 µl of Mueller Hinton Broth culture medium or Nutrient Broth was poured in sterile conditions in all the wells under, then 100 µl of the initial stock prepared in the previous step was poured into the first well and it is diluted by serial dilution method. At the end, 10 µl of bacteria prepared in half McFarland dilution was added to all the wells and incubated for 24 h. Then it was measured by direct observation with eyes and optical measurement of concentration with Eliza rider device. To determine MBC using the MIC value obtained in the previous step, the dilutions before and after the MIC sample were cultured in tubes containing liquid culture medium (broth) and heated for 24 h. Then the tube was cultured in a solid culture medium (agar) under sterile conditions and incubated again for 24 h at 37 ºC. Finally, MBC was determined for the samples.

3. Results and discussion

3.1 Nanostructures

The IR absorption spectra of graphene/MOF-5 nanocomposites were recorded in the range of 400–4000 cm^{-1} with KBr pellets. FTIR spectra of samples shows in different concentration of BDC ligand (Fig. 1). The O–H stretching vibrations peaks can be observed around 3200–3500 cm^{-1}. The peak around 2929 cm^{-1} is duo to the sp^3 C–H bonding. The strong peaks around 1650–1720 cm^{-1} are characteristic to the symmetric and asymmetric stretching of C-O bonds. It can be attributed to the benzene ring present in BDC linker ligand and also presence of graphene oxide in the samples. The peak around 1255 cm^{-1} shows the stretching of the aromatic C-H groups of the benzene ring in BDC ligand. The peaks around 1392 and 865 cm^{-1} are because of the in-plane and out of the plane stretching of the aromatic C-H groups of the benzene ring present in terephthalic acid. Presence of these peaks were reported frequently in published papers on synthesize the MOF-5 nanostructures [2–5, 81]. Furthermore, the peak at 1093 cm^{-1} is the characteristic peak of graphene-based materials corresponds to C-O bonds [82]. Fourier transform infrared spectrum of samples is consistent with the reported results on synthesized MOF-5 nanostructures [20, 64, 83]. Intensity of FTIR peaks was increased from sample a to c with the amount of ligand in the liquid environment due to increase the number of synthesized nanostructures in the suspensions.

XRD patterns of samples were recorded by drying a few drops of the suspension on a silicon substrate under low dose conditions in the liquid. X-ray diffraction of samples is shown in figure 2 from 2θ=5° to 80°. The peaks at 2θ=15-30° present the crystalline structure of MOF-5 according to the previously reported pattern [64]. Review of the published results on MOF-5 nanostructures which were produced by chemical methods shows that the XRD peaks of this complex nanomaterial often occur at 2θ=5-20° [2, 3]. While the peaks of XRD patterns of the MOF-5 nanostructures which were produced by PLA method occur at 2θ=15-30° [34, 64]. The main reason for shift of the position of XRD peaks is the variation of lattice parameters of the material. With decreasing (increasing) the distance between successive, parallel planes of atoms in the lattice structure of material the XRD peaks shift toward larger (smaller) angles. Formation of laser ablation produced nanostructure in the high-pressure plasma plume on the surface of the target during the laser ablation process, compresses their lattice structure which leads to a right shift the position of their XRD peaks.

TEM images (Figs. 4) show that graphene nanosheets are very thin and transparent. The number of reflected X-ray photons from thin nanosheets are so low that they do not make any noticeable peaks. Lack of observation of graphene peak in X ray diffraction pattern of nanomaterials has been reported frequently [75–77].

Based on the results, samples have crystalline cubic structure in different ligand concentration. Also, the increase of peak intensity is due to the increase of ligand concentration. With increasing the concentration of ligand in the liquid environment, number of synthesized nanocomposites in a grain was increased which in turn leaded to increase the intensity of XRD peaks. XRD result show that the amount of ligand in the liquid environment is not affective on the lattice structure of nanocomposites.

The size and morphology of the samples were determined by field emission scanning electron microscope images in two scales in Figs. 3. Based on the results, the structures are cubic shapes with smooth surfaces in the range of nanometers. Also, increasing the concentration causes their anisotropic growth and formation of nanorods. The number of nanos-

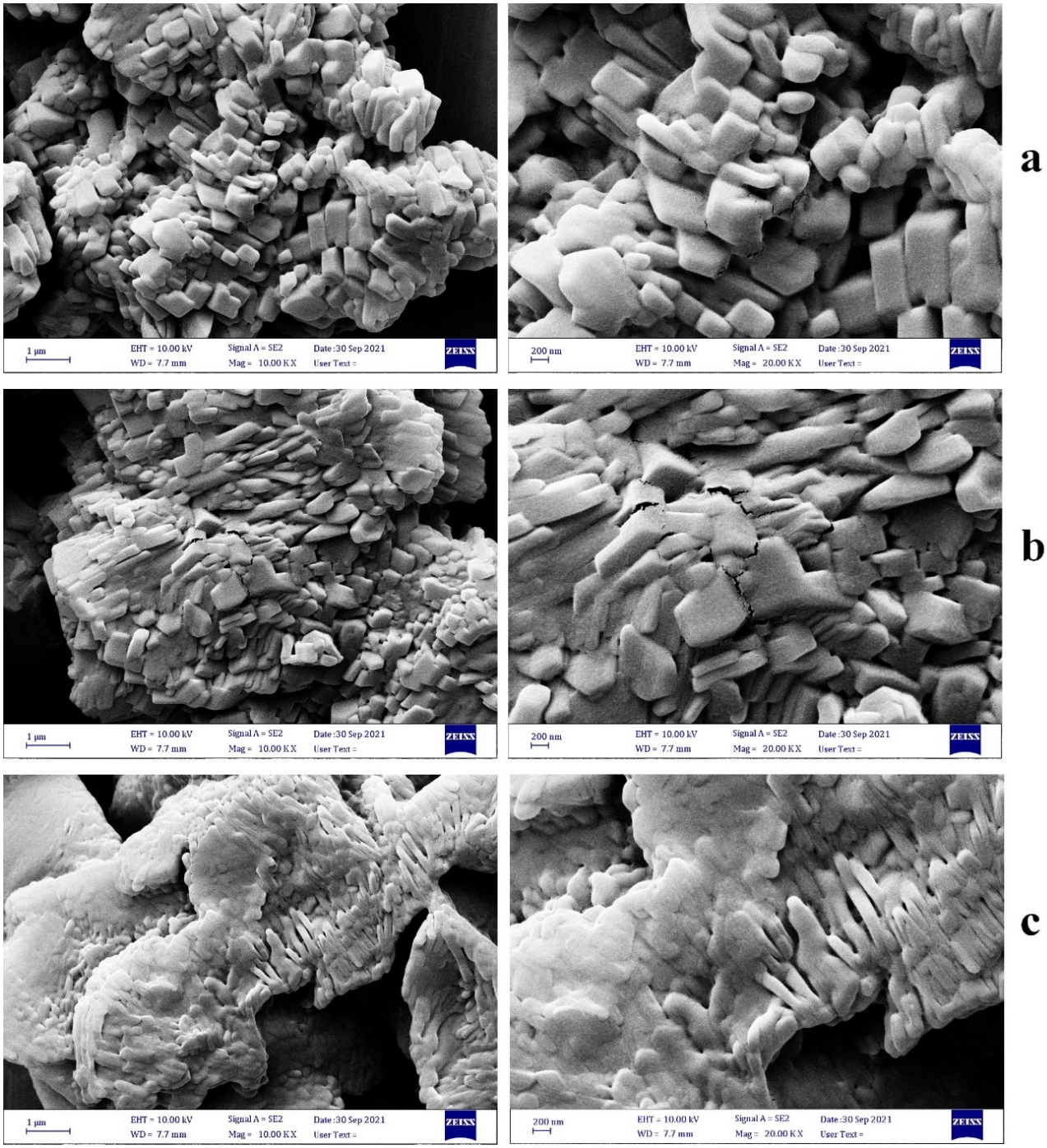

Figure 3. FESEM images of graphene/MOF-5 nanocomposites at different BDC ligand concentrations a) 0.328, b) 0.631, and c) 1.234 g.

tructures increased significantly with increasing the ligand concentration in the liquid medium. Increasing the intensity of XRD peaks of samples a to c is in good agreement with size of produced nanostructures in FESEM pictures. Furthermore, adhesion of nanostructures was increased significantly with increasing the amount of ligand in the liquid environment. In sample c cubes were adhere to each other to form a micron size un-uniform structure. Concentration of MOFs is so high that the graphene nanosheets cannot be distinguished. But presence of graphene nanosheets in the structure of synthesized nanostructures is the main responsible for their different morphology with produced MOF-5 nanostructures which was reported in our former work [64]. Production of MOF-5 nanostructures with similar morphology by PLA method has not been reported so far but chemically produced MOF-5 nanostructures in the presence of surfactant has almost the similar morphology [2].

Transmission electron microscope images of the samples are presented in figures. 4 with two different magnifications. In these images, graphene nanosheets are observable in the form of transparent large surfaces. Sides of them differs between 1 to 5 micrometers. Their transparency confirm that

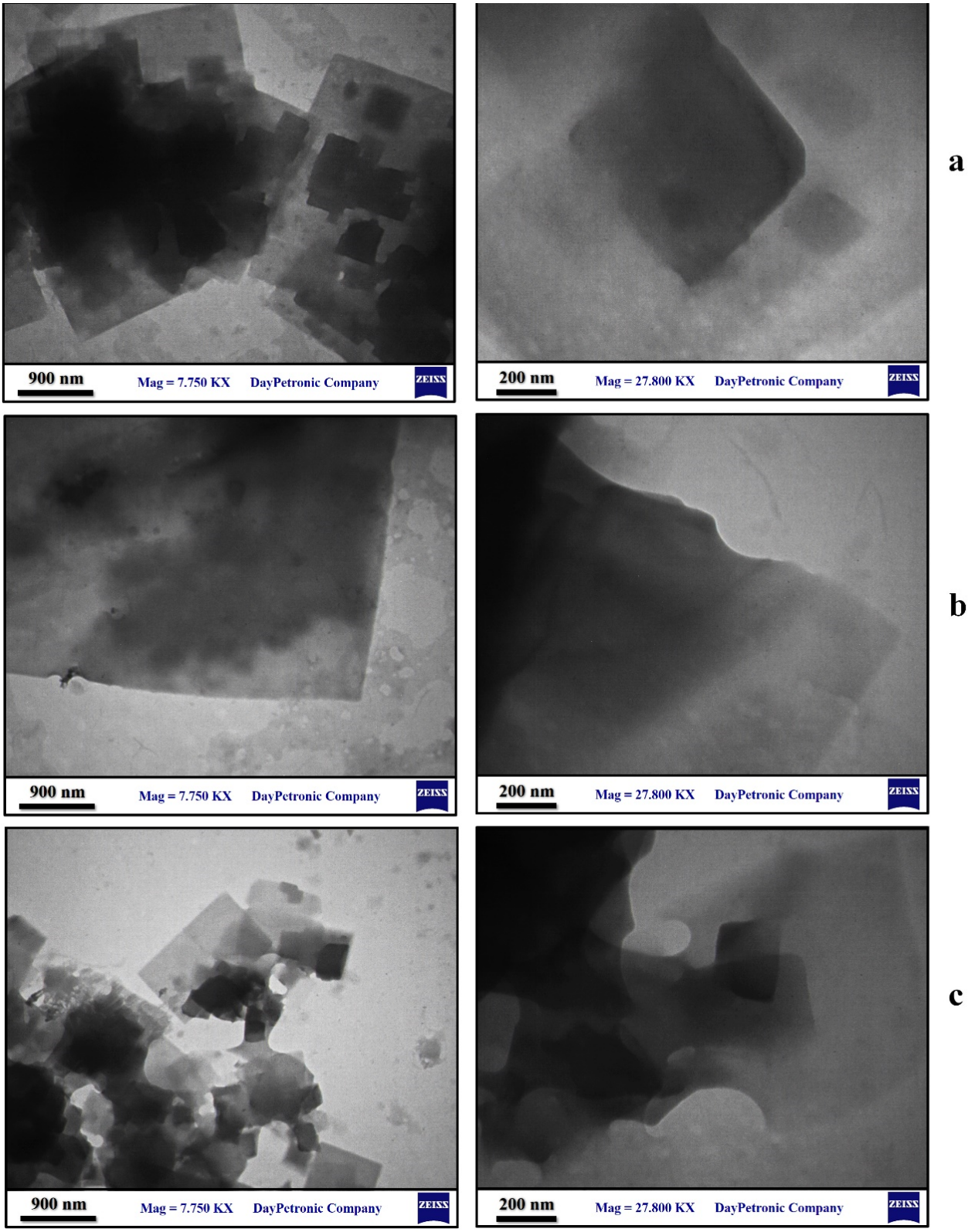

Figure 4. TEM images of graphene/MOF-5 nanocomposites at different BDC ligand concentrations a) 0.328, b) 0.631, and c) 1.234 g.

they are few layers graphene [67–69]. With increasing the density of the ligand in the liquid environment of ablation, size of graphene nanosheets was decreased. Size of PLA produced nanostructures strongly depends on the density of the liquid environment. With increasing the density of liquid environment, the pressure of plasma plume on the surface of target during the ablation increases. The higher the pressure of the plasma, the smaller the size of synthesized nanostructures. Furthermore, TEM images show the nanometer sized and cubic MOF-5 crystals which are lo-

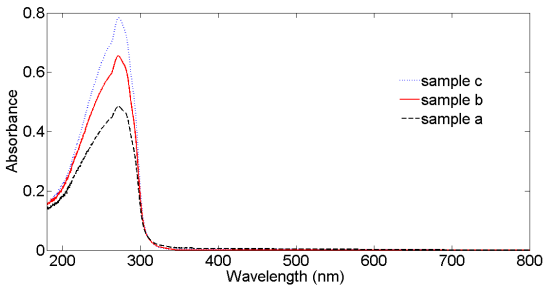

Figure 5. UV–Vis-NIR absorption spectra of graphene/MOF-5 nanocomposites at different BDC ligand concentrations a) 0.328, b) 0.631, and c) 1.234 g.

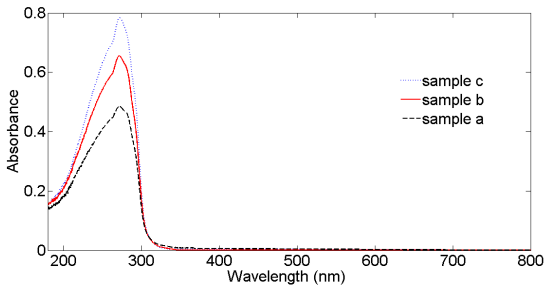

Figure 6. Tauc plot to extract the bandgap energy of the synthesized graphene/MOF-5 nanocomposites, produced with different BDC ligand concentrations a) 0.328, b) 0.631, and c) 1.234 g.

cated on the surface of graphene nanosheets. Concentration and adhesion of MOF cubes was increased with increasing the density of BDC ligand in the liquid environment while their uniformity was decreased. These results confirm the results of FESEM images and X-ray diffraction patterns of samples. In fact, all MOF-5 nanomaterials, produced by any method, are cubic [2, 3, 64].

UV–Visible-NIR absorption spectra of synthesized graphene nanosheets decorated MOF-5 nanostructures are presented in Fig. 5. Spectra were recorded from the produced suspensions in 1 cm quartz cuvettes. The absorption spectra were peaked widely at about λ_{max}=260-270 nm for the samples with concentration of a) 0.328, b) 0.631, and c) 1.234 g of BDC ligand. From one side of view graphene oxide and graphene nanosheets have an absorption peak at 230 nm and a small shoulder at 300 nm correspond to the π-π^* transition of aromatic C–C bonds and the n-π^* transition of C=O bonds, respectively [67–69]. From another side of view, absorption peak of MOF-5 is a wide band peaked widely at λ = 255–300 nm. This band includes the π-π^* transition of the organic ligand absorption peak and the excitonic absorption peak of free ZnO nanoparticles [64]. The absorption peak of synthesized graphene/MOF-5 is the overlap of graphene and MOF-5 absorption peaks. Increasing the intensity of peaks from sample a to c is due to increase the amount of the concentration of synthesized nanostructures in the suspensions while the small red shift of the absorption peaks is due to increase in their size. Similar results on the absorption spectrum of MOF-5 nanostructures were observed in our previous works [64].

Optical bandgap of nanostructures is an important parameter to distinguish their photocatalytic activities. Tauc method was employed to extract the optical bandgap of synthesized graphene/MOF-5 nanostructures. Tauc method was described in former published works [67–69]. Results are plotted in Fig. 6. In this figure variation of $(\alpha h\nu)^2$ versus $h\nu$, correspond to direct allowed transition, has been shown. h is the Planck's constant. α and ν are the absorption coefficient of samples and the photon frequency respectively. On the Tauc plot, the extrapolating of the linear part of the graph at the absorption edge region to the abscissa yields the energy of the optical bandgap of the material. Results show that although there are several differences between the synthesized nanocomposites but their bandgap energies are almost equal to 4.1 eV. Bandgap energy of nanostructures depends on their materials, and size. Equal magnitudes of bandgap energy confirm that for produced graphene/MOF-5 nanocomposites, effect of size was covered by the effect of graphene amount in the composition. This result is consistent with our previous report for MOF-5 without composition with graphene [64].

3.2 Antibacterial activity

The minimum bactericidal concentration and minimum inhibitory concentration were used for antibacterial activity of the samples. Staphylococcus aureus and Escherichia coli were grown overnight at 37 °C in Mueller Hinton Broth (MHB) medium. Serial dilutions of doubling agents were added to 100 μl titer plates, followed by 100 μl of bacteria for a final inoculation of 5×10^5 colony forming units (CFU) / ml. The plates were incubated at 37 °C for 24 h and MICs were determined. Then, 100 μl of the 24 hour inhibitory concentration test sample and most concentrations were placed in MHA medium and incubated at 37 °C overnight to determine MBC. The MIC and MBC results of

Table 1. MIC and MBC of samples.

Ligand content (gr)	Strains			
	E. coli (ATCC 25922)		*S. aureus* (ATCC 25923)	
	MIC (µg/ml)	MBC (µg/ml)	MIC (µg/ml)	MBC (µg/ml)
0.328	0.5	1	1	1
0.631	0.5	0.5	0.25	0.5
1.234	0.125	0.5	0.125	0.125

two bacteria are presented in Table 1. According to the ratio MBC/MIC, the antibacterial activity was evaluated. If the ratio MBC/MIC$\leq$4, the effect was considered as bactericidal but if the ratio MBC/MIC>4, the effect was defined as bacteriostatic. Based on the results, the samples are bactericidal. The main mechanisms of MOF antibacterial activity are: direct contact with cell walls and destruction of bacterial cells, production of reactive oxygen species (ROS) and release of antimicrobial ions, mainly Zn^{+2} ions [84]. In this study, the effective factors on antibacterial activity can be the release of Zn^{+2} ions and zinc from metal centers and carboxyl group of linkers of the MOF. In general, more antibacterial properties can be observed for Escherichia coli due to the gravity of the opposite charges. According to the results, increasing the concentration of the ligand and the size of the nanostructure has reduced its antibacterial properties. Similar results on the inhibition zone of MOF-5 nanostructures prepared by hydrothermal method were reported by Hu et. al [85].

4. Conclusion

Pulsed laser ablation method was employed to synthesis graphene decorated MOF-5 nanocomposites in liquid environment for the first time. The MOF was fabricated by self-assembly of ablated Zn^{2+} ion as a connector and BDC ligand as a bridging ligand. Variety of spectroscopic and microscopic diagnostics were used to evaluate of the synthesized nanostructures. Results show that ligand concentration has an effective role in the morphology, size and concentration of produced samples by PLA method. FTIR results identified the basic functional groups of MOF-5 nanostructures in different ligand concentration. XRD patterns confirmed the cubic crystalline structure of MOF-5. FESEM images illustrated the unique morphology of graphene/MOF-5 nanocomposites which is very different from PLA produced MOF-5 nanostructures. TEM images confirmed that MOF-5 nanostructures were located on the surface of surface of the few layer transparent graphene nanosheets.

Furthermore, the antibacterial properties of graphene/MOF-5 nanocomposites against Staphylococcus aureus (gram positive) and Escherichia coli (gram negative) bacteria were investigated. At this stage stronger antibacterial effects were observed against the gram-negative bacteria due to their gravitation of opposite charges.

Overall, by increasing the ligand concentration in the liquid environment of laser ablation, the size of synthesized nanostructures was increased which in turn leaded to decrease their antibacterial properties.

In the continuation of researches on the capabilities of pulsed lasers ablation in the field of nanomaterials processing, these results also corroborate on the role of laser ablation method as an easy and short time method to synthesize the complex structure nanomaterials.

Conflict of interest statement

The authors declare that they have no conflict of interest.

References

[1] Q. L. Zhua and Q. Xu. *Chem. Soc. Rev.*, **43**:5468, 2014.

[2] K. A. S. Usman, J. W. Maina, S. Seyedin, M. T. Conato, L. M. Payawan, L. F. Dumée, and J. M. Razal. *NPG Asia Materials*, **12**:58, 2020.

[3] F. Ghourchian, N. Motakef-Kazemi, E. Ghasemi, and H. Ziyadi. *J. Environ. Chem. Eng.*, **76**:106388, 2021.

[4] G. Ferey. *Chem. Soc. Rev.*, **37**:191, 2008.

[5] B. Miri, N. Motakef-Kazemi, S. A. Shojaosadati, and A. Morsali. *Iran. J. Pharm.*, **17**:1164, 2018.

[6] O. R. Evans and W. Lin. *Chem. Mater.*, **13**:2705, 2001.

[7] V. Stavila, A. A. Talin, and M. D. Allendorf. *Chem. Soc. Rev.*, **43**:5994, 2014.

[8] M. Oh and C. A. Mirkin. *Chem. Int. Ed.*, **45**:5492, 2006.

[9] H. Sun, S. Cong, Z. Zheng, Z. Wang, Z. Chen, and Z. Zhao. *J. Am. Chem. Soc.*, **141**:870, 2019.

[10] A. Chidambaram and K. C. Stylianou. *Inorg. Chem. Front.*, **5**:979, 2018.

[11] X. Fang, B. Zong, and S. Mao. *Nano-Micro Lett.*, **10**:64, 2018.

[12] M. S. Alhumaimess. *J. Saudi Chem. Soc.*, **24**:461, 2020.

[13] N. M. Musyoka, J. Ren, H. W. Langmi, B. C. North, M. Mathe, and D. Bessarabov. *J Alloy Compd.*, **724**:450, 2017.

[14] H. Zhu, Q. Zhang, and S. Zhu. *ACS Appl. Mater. Interfaces.*, **8**:17395, 2016.

[15] B. Chen, L. Wang, F. Zapata, and G. Qian. *J. Am. Chem. Soc.*, **130**:6718, 2008.

[16] J. Dong, D. Zhao, Y. Lu, and W. Y. Sun. *J. Mater. Chem. A.*, **7**:22744, 2019.

[17] S. Jensen, K. Tan, W. Lustig, D. Kilin, J. Li, Y. J. Chabal, and T. Thonhauser. *J. Mater. Chem. C.*, **7**:2625, 2019.

[18] S. Hajiashrafi and N. Motakef-Kazemi. *Heliyon.*, **5**:e02152, 2019.

[19] N. Motakef-Kazemi, M. Rashidian, S. Taghizadeh Dabbagh, and M. Yaqoubi. *IJCCE.*, **40**:11, 2020.

[20] M.R. Mehmandoust, N. Motakef-Kazemi, and F. Ashouri. *Iran. J. Sci. Technol. A.*, **43**:443, 2019.

[21] N. Motakef-Kazemi. *AMEC J.*, **2**:67, 2019.

[22] G. Wyszogrodzka, B. Marszałek, B. Gil, and P. Dorożyński. *Drug Discov.*, **21**:1009, 2016.

[23] N. Stock and S. Biswas. *Chem. Rev.*, **112**:933, 2012.

[24] N. Motakef-Kazemi, S. A. Shojaosadati, and A. Morsali. *Micropor Mesopor Mat.*, **186**:73, 2014.

[25] N. Motakef-Kazemi, S. A. Shojaosadati, and A. Morsali. *J Iran Chem Soc.*, **13**:1205, 2016.

[26] O.M. Yaghi and H. Li. *J. Am. Chem. Soc.*, **117**:10401, 1995.

[27] Z. Wang, Z. Li, M. Nga, and P.J. Milner. *Dalton Trans.*, **49**:16238, 2020.

[28] H. Al-Kutubi, J. Gascon, E. J. R. Sudhölter, and L. Rassaei. *Chem Electro Chem.*, **2**:462, 2015.

[29] J. Klinowski, F. A. Almeida Paz, P. Silva, and J. Rocha. *Dalton Trans.*, **40**:321, 2011.

[30] S. H. Jhung, J. H. Lee, J. W. Yoon, C. Serre, G. Ferey, and J. S. Chang. *Adv Mater.*, **19**:121, 2007.

[31] W. J. Son, J. Kim, J. Kim, and W. S. Ahn. *Chem Commun.*, **47**:6336, 2008.

[32] Y. Chen, C. Yang, X. Wang, J. Yang, K. Ouyang, and J. Li. *J. Mater. Chem. A.*, **4**:10345, 2016.

[33] J. H. Liao, P. C. Wu, and W. C. Huang. *Cryst Growth Des.*, **6**:1062, 2006.

[34] F. Ataei, D. Dorranian, and N. Motakef-Kazemi. *JTAP.*, **14**:1, 2020.

[35] S. L. Campello, G. Gentil, S. A. Júnior, and W. M. de Azevedo. *Mater.*, **148**:200, 2015.

[36] O. Maria Menezes Madeiro da Costa and W.M. de Azevedo. *J. Lumin.*, **170**:648, 2016.

[37] H. Li, M. Eddaoudi, M. O'Keeffe, and O. Yaghi. *Nature.*, **402**:276, 1999.

[38] G. Chen, J. Luo, M. Cai, L. Qin, Y. Wang, L. Gao, P. Huang, Y. Yu, Y. Ding, X. Dong, X. Yin, and J. Ni. *Molecules.*, **24**:3369, 2019.

[39] J. B. Bates. *Acta A.*, **27**:1255, 1971.

[40] W. Kukulka, K. Cendrowski, B. Michalkiewicz, and E. Mijowska. *RSC Adv.*, **9**:18527, 2019.

[41] N. Bakhtiari and S. Azizian. *ACS Omega.*, **3**:16954, 2018.

[42] O. Guselnikova, P. Postnikov, R. Elashnikov, E. Miliutina, V. Svorcik, and O. Lyutakov. *Anal. Chim. Acta.*, **1068**:70, 2019.

[43] W. Kleist, M. Maciejewski, and Al. Baiker. *Thermochim. Acta.*, **499**:71, 2010.

[44] V. I. Isaeva, O. P. Tkachenko, I. V. Mishin, G. I. Kapustin, A. A. Kostin, K. V. Klementiev, and L. M. Kustov. *Stud Surf Sci Catal.*, **174**:463, 2008.

[45] J. Li, S. Cheng, Q. Zhao, P. Long, and J. Dong. *Int. J. Hydrog. Energy.*, **34**:1377, 2009.

[46] N. Jiang, Z. Deng, S. Liu, C. Tang, and G. Wang. *Korean J Chem Eng.*, **33**:2747, 2016.

[47] A. Parkash. *ECS J Solid State Sci Technol.*, **9**:075002, 2020.

[48] S. Amirjalayer and R. Schmid. *Micropor Mesopor Mat.*, **125**:90, 2009.

[49] C. Xu, J. Yang, M. Veenstra, A. Sudik, J. J. Purewal, Y. Ming, B. J. Hardy, J. Warner, S. Maurer, U. Mueller, and D. J. Siegel. *Int. J. Hydrog. Energy.*, **38**:3268, 2013.

[50] P. Kumar, A. Deep, A. K. Paul, and L. M. Bharadwaj. *J Porous Mater.*, **21**:99, 2014.

[51] S. Bordiga, C. Lamberti, G. Ricchiardi, L. Regli, F. Bonino, A. Damin, K. P. Lillerud, M. Bjorgen, and A. Zecchin. *Chem. Commun.*, **20**:2300, 2004.

[52] Z. Karimzadeh, S. Javanbakht, and H. Namazi. *Bioimpacts.*, **9**:5, 2019.

[53] N. Bhardwaj, S. K. Pandey, J. Mehta, S. K. Bhardwaj, K. H. Kim, and A. Deep. *Toxicol Res (Camb).*, **7**:931, 2018.

[54] G. L. Denisov, P. V. Primakov, A. A. Korlyukov, V. V. Novikov, and Y. V. Nelyubina. *J. Coord. Chem.*, **45**:836, 2019.

[55] C. McKinstry, R. J. Cathcart, E. J. Cussen, A. J. Fletcher, S. V. Patwardhan, and J. Sefcik. *Chem. Eng. J.*, **285**:718, 2016.

[56] J. Yong Choi, J. Kim, S. Hwa Jhung, H. K. Kim, J. J. S. Chang, and H. K. Chae. *Bull. Korean Chem. Soc.*, **27**:1523, 2006.

[57] J. K. Choi, J. Kim, S. H. Jhung, H. K. Kim, J. S. Chang, and H.K. Chae. *Bull Kor Chem Soc.*, **27**:1523, 2006.

[58] Y. Wang, S. Ge, W. Cheng, Z. Hu, Q. Shao, X. Wang, J. Lin, M. Dong, J. Wang, and Z. Guo. *Langmuir.*, **36**:9658, 2020.

[59] Hm. Yang, X. Lu, X. Song, T. Yang, Zh. Liang, and Cm. Fan. *Trans. Nonferrous Met. Soc. China.*, **25**:3987, 2015.

[60] D. J. Tranchemontagne, J. R. Hunt, and O. Yaghi. *Tetrahedron.*, **64**:8553, 2008.

[61] R. Ye, M. Ni, Y. Xu, H. Chen, and S. Li. *RSC Adv.*, **8**:26237, 2018.

[62] D. Lv, Y. Chen, Y. Li, R. Shi, H. Wu, X. Sun, J. Xiao, H. Xi, Q. Xia, and Z. Li. *J. Chem. Eng. Data.*, **62**:2030, 2017.

[63] R. Sabouni, H. Kazemian, and S. Rohani. *Chem. Eng. J.*, **165**:966, 2010.

[64] F. Ataei, D. Dorranian, and N. Motakef-Kazemi. *J. Mater. Sci.: Mater. Electron.*, **32**:3819, 2021.

[65] L. Malik and A. Escarguel. *Europhys. Lett.*, **124**:64002, 2019.

[66] L. Malik. *Opt. Laser Technol.*, **132**:106485, 2020.

[67] L. Malik, A. Escarguel, M. Kumar, A. Tevatia, and R. Singh Sirohi. *Laser Phys. Lett.*, **18**:086003, 2021.

[68] H.K. Malik. *Physics Letters A.*, **384**:12630, 2020.

[69] D. Sharma, D. Singh, and H. K. Malik. *Plasmonics.*, **15**:177, 2020.

[70] H.K. Malik and S. Punia. *Phys. Plasmas.*, **26**:063102, 2019.

[71] H. K. Malik. *Laser-Matter Interaction for Radiation and Energy*. CRC Press, 1th edition, 2021.

[72] X. Li, J. Yu, S. Wageh, A. A. Al-Ghamdi, and J. Xie. *Small*, **12**:6640, 2016.

[73] W. Choi, I. Lahiri, R. Seelaboyina, and Y. Soo Kang. *Solid State Mater. Sci.*, **35**:52, 2010.

[74] G. Kumar and D.T. Masram. *ACS Omega.*, **6**:9587, 2021.

[75] E. Vaghri, D. Dorranian, and M. Ghoranneviss. *Mater. Chem. Phys.*, **203**:235, 2018.

[76] E. Solati and D. Dorranian. *Appl. Phys. B.*, **122**:76, 2016.

[77] N. Ebrahim Jasbi, E. Solati, and D. Dorranian. *J. Alloys Compd.*, **861**:157956, 2021.

[78] Y. Choi, S. Won Song, W. Hooch Antink, H. Min Kim, and Y. Piao. *Chem. Commun.*, **53**:10108, 2017.

[79] P. Garg, Bharti, R.K. Soni, and R. Raman. *J. Mater. Sci. Mater.*, **31**:1094, 2020.

[80] G. Ding, S. Xie, Y. Liu, L. Wang, and F. Xu. *Appl. Surf. Sci.*, **345**:310, 2015.

[81] F. Haftan and N. Motakef-Kazemi. *Nanomed Res J.*, **6**:1, 2021.

[82] F. Tuz Johra, J.W. Lee, and W.G. Jung. *J Ind Eng Chem.*, **20**:2883, 2014.

[83] Z. Çiplak, N. Yildiz, and A. Çalimli. *Fuller. Nanotub. Car N.*, **3**:361, 2014.

[84] A. Sirelkhatim, S. Mahmud, A. Seeni, N. H. M. Kaus, L.C. Ann, S. K. M. Bakhori, H. Hasan, and D. Mohamad. *Nano-Micro Lett.*, **7**:219, 2015.

[85] Y. Hu, H. Yang, R. Wang, and M. Duan. *Nano-Micro Lett.*, **7**:219, 2015.